Supplementary Information

Design of Fe, N co-doped multi-walled carbon nanotubes for efficient oxygen reduction

Peng Du [a,b,c,†], Yan Bao [a,d,†], Chen Guo [c,†], Lawrence WU [c], Jie Pan [a,b,c], Chenghao Zhao [a,b,c], Fei-Xiang Ma [a,b,c,d,], Jian Lu [a,c,d,e,*], Yang Yang Li [a,b,c,d,e,*]*

[a] *Hong Kong Branch of National Precious Metals Material Engineering Research Centre (NPMM), City University of Hong Kong, Kowloon, Hong Kong, P.R. China*

[b] *Center of Super-Diamond and Advanced Films (COSDAF), City University of Hong Kong, Kowloon, Hong Kong, P.R. China*

[c] *Department of Material Science and Engineering, City University of Hong Kong, Kowloon, Hong Kong, P.R. China*

[d] *Department of Mechanical Engineering, City University of Hong Kong, Greater Bay Joint Division, Shenyang National Laboratory for Materials Science, Tat Chee Avenue, Kowloon, Hong Kong, P.R. China*

[e] *Center for Advanced Structural Materials, City University of Hong Kong Shenzhen Research Institute, Greater Bay Joint Division, Shenyang National Laboratory for Materials Science, 8 Yuexing 1st Road, Shenzhen Hi-Tech Industrial Park, Nanshan District, Shenzhen, P.R. China*

*Corresponding Author: *E-mail: mfx1989@gmail.com (Fei-Xiang Ma); *E-mail: jianlu@cityu.edu.hk. (Jian Lu); *E-mail: yangli@cityu.edu.hk. (Yang Yang Li)*

[†] *These authors contributed equally.*

Experimental

Chemicals

Multi-walled carbon nanotubes (MWCNTs) and single-walled carbon nanotubes (SWCNTs) were purchased from Tanfeng Tech. Inc. (China). 20 wt.% commercial platinum/carbon (Pt/C) and melamine were purchased from Sigma-Aldrich (USA). Nafion solution (5 wt.% in alcohol and water) was obtained from DuPont (USA). Potassium hydroxide (KOH, ≥ 98%), nitric acid (HNO_3, ≥ 65%), hydrochloric acid (HCl, ≥ 37%), sulfuric acid (H_2SO_4, ≥ 98%), methanol (CH_3OH, ≥ 99.8%) and isopropanol ($(CH_3)_2CHOH$, ≥ 99.5%) were purchased from Honeywell (USA). Iron chloride hexahydrate ($FeCl_3 \cdot 6H_2O$, ≥ 97%) was purchased from J&K Chemicals (China).

Catalyst synthesis

Initially, multi-walled carbon nanotubes (MWCNTs) or single-walled carbon nanotubes (SWCNTs) (1.0 g) were dispersed in 40 ml of concentrated HNO_3 in a flask and continuously stirred at 70 °C for 24 h. The solution was centrifuged at 8,000 rpm. The collected solid was washed with deionized water several times. The obtained oxidized MWCNTs or SWCNTs was then immersed into 40 ml of 1.0 wt.% $FeCl_3$ solution and continuously stirred at room temperature for 24 h. Subsequently, the dispersed solution of MWCNTs or SWCNTs and Fe^{3+} was freeze-dried. Then, the above sample, together with the same amount of melamine, was annealed under nitrogen at 800°C, 900 °C or 1000°C. Melamine ($C_3H_6N_6$) is a cheap industrial product with an ultrahigh nitrogen content (66.6 wt.%). During the heat treatment, the melamine can decompose to CN-rich vapor, which would be subsequently reacted with Fe^{3+} adsorbed MWCNTs to form unique Fe,N-MWCNTs, and therefore a rather ideal choice for nitrogen source compared with corrosive and environmentally unfriendly gas nitrogen source (NH_3). The placing arrangement of samples in the tube furnace was in the way shown in Figure 1a. For purification (to remove metal nanoparticles or clusters), the sample was sonicated in 0.1 M HCl for 30 mins, and was then dried in an oven at 80 °C overnight. The resultant catalyst was

denoted as Fe,N-MWCNTs-X or Fe,N-SWCNTs-X, where X represents the annealing temperature. N-MWCNTs was prepared by a similar method as above except that no iron source was added. The catalyst with no temperature indicated in this study are all referred to as the catalyst prepared at 900 °C.

Material characterizations

Scanning electron microscopy (SEM) measurements were performed using a field emission scanning electron microanalyzer (Philips XL-30). Transmission electron microscopy (TEM) images were obtained on a JEM-2100F microscope (JEOL). X-ray photoelectron spectroscopic (XPS) measurements were carried out on an X-ray photoelectron spectrometer (VG ESCALAB 220i-XL). The specific surface areas, pore sizes and pore volumes were measured using a N_2 adsorption desorption analyzer (Quantachrome Nova 1200e). The X-ray diffraction patterns (XRD) of the products were recorded on an X-ray diffractometer (Bruker D2 Phaser). Raman spectra were obtained with a laser excitation at 632.8 nm by an inVia-Refiex spectrometer (Renishaw 2000). The accurate mass of iron was measured by inductively coupled plasma-atomic emission spectrometer (ICP-AES) (PE 2100DV).

Electrochemical measurements

Electrochemical measurements were performed in a conventional three-electrode cell using a CHI 660 workstation (CH Instruments). A glassy carbon (GC) disk with a diameter of 5.0 mm was used as the substrate for the working electrode. For each sample, 5.0 mg of the sample was ultrasonically dispersed in the mixed solution of 480 μL isopropanol and 20 μL of 5 wt.% Nafion aqueous solution for 30 minutes. Then, about 12 μL of this suspension was added dropwise and adhered to the GC rotating disk electrode (RDE, 5 mm diameter) or rotating ring-disk electrode (RRDE, 4.93 mm inner diameter and 5.38 mm outer diameter), and then air dried naturally, fixed with a total loading mass of about 0.6 $mg \cdot cm^{-2}$. For comparison, 20 wt.% commercial Pt/C powder (Sigma-Aldrich) was tested under identical conditions, with a loading of 0.25 mg cm^{-2}. A saturated calomel electrode (SCE) was used as a reference electrode, and a

platinum wire for alkaline electrolyte or a graphitic rod (Φ = 0.8 cm) for acidic electrolyte was used as a counter electrode. All potential values reported in this study were converted to the reversible hydrogen electrode (RHE) scale, according to the equation:

$$E_{RHE} = E_{SCE} + 0.0591\text{pH} + 0.242$$

Cyclic voltammetry (CV) curves were obtained in nitrogen and oxygen saturated electrolytes, respectively, with a sweep rate of 50 $mV \cdot s^{-1}$. RDE/RRDE linear sweep voltammetry (LSV) measurements were carried out in 0.1M KOH/0.5M H_2SO_4 solution saturated with O_2 with a scanning rate of 10 $mV\ s^{-1}$ at rotating speeds of 1600 rpm. LSV curves at different rotating speeds from 400 rpm to 2400 rpm (400 rpm per interval) of the catalyst using a rotating disk electrode (RDE) were also conducted for understanding the electron transfer kinetics. The Koutecky-Levich (K-L) plots were analyzed at various electrode potentials. According to the K-L equation as follows, the slopes of the linear t-lines was used to calculate the number of electrons transferred (n):

$$1/J = 1/J_K + 1/J_L = 1/J_K + 1/(B\omega^{1/2})$$

where J is the measured current density, J_K and J_L are the kinetic and limiting current densities, respectively, and ω is the electrode rotation rate. The theoretical value of the Levich slope (B) is evaluated from the following equation:

$$B = 0.62nFC_0D_0^{2/3}V^{-1/6}$$

where n is the total electron transfer number during oxygen reduction, F is the Faraday constant (96485 C mol^{-1}), C_0 (1.2×10^{-6} mol cm^{-3} in 0.1 M KOH) is the bulk concentration of O_2, D_0 (1.9×10^{-5} cm^2s^{-1} in 0.1 M KOH) represents the diffusion coefficient of O_2, and V (0.01 $cm^2\ s^{-1}$ in 0.1 M KOH) corresponds to the kinematic viscosity of the electrolyte.

The hydrogen peroxide yield [H_2O_2 (%)] and the electron transfer number (n) were calculated from the data of rotating ring-disk electrode (RRDE) tests by the following two equations:

$$H_2O_2\,(\%) = 200\times(I_R/N)/(I_R/N+I_D)$$

$$n = 4\times I_D/(I_R/N+I_D)$$

where I_D represents to the disk current, I_R represents the ring current, and N is the ring collection coefficient (N = 0.37).

Computational Details

All calculations were carried out by spin-polarized DFT with the Vienna *Ab initio* Simulation Package (VASP) [S1]. Electron exchange-correlation was expressed by the Perdew-Burke-Ernzerh of (PBE) functional within the generalized gradient approximation (GGA) [S2]. To describe the ionic cores, the projector augmented wave (PAW) pseudopotential was applied [S3]. The Monkhorst-Pack K-points were set to be 5 × 5 × 1 during geometry optimization. The plane wave energy cutoff, and convergence criterion for electronic energy and forces were set as 500 eV, 10^{-5} eV, and 0.02 eV/Å, respectively. The van der Waals (vdW) interactions were taken into consideration by using the Grimme method (DFT-D3). The calculated lattice parameters are 9.84 × 9.84 × 20 Å in this work.

The computational hydrogen electrode (CHE) model was used to calculate the change in Gibbs free energy (ΔG) [S4, S5]. In CHE model, $H^+ + e^- \rightleftharpoons 1/2\ H_2(g)$ was equilibrated at 0 V *vs* the reversible hydrogen electrode (RHE) at all pH values. Free energies (G) of each state were obtained by the expression,

$$G = E + ZPE + \int C_P dT - TS + G_{pH} \quad (3)$$

where T is temperature, E is electronic energy. ZPE, $\int C_P dT$, and TS are the zero point energy, enthalpy change from 0 to T K contributed by molecular vibration, and entropy correction, which are obtained based on vibration analysis at 298.15 K. G_{pH} is the free energy correction of pH, which can be calculated by $G_{pH} = k_B T \ln 10 \times pH$. In this work, pH value was set as 0 and 14, respectively. The equilibrium potential of ORR is 1.23 V for acidic condition and 0.401 V for alkaline condition.

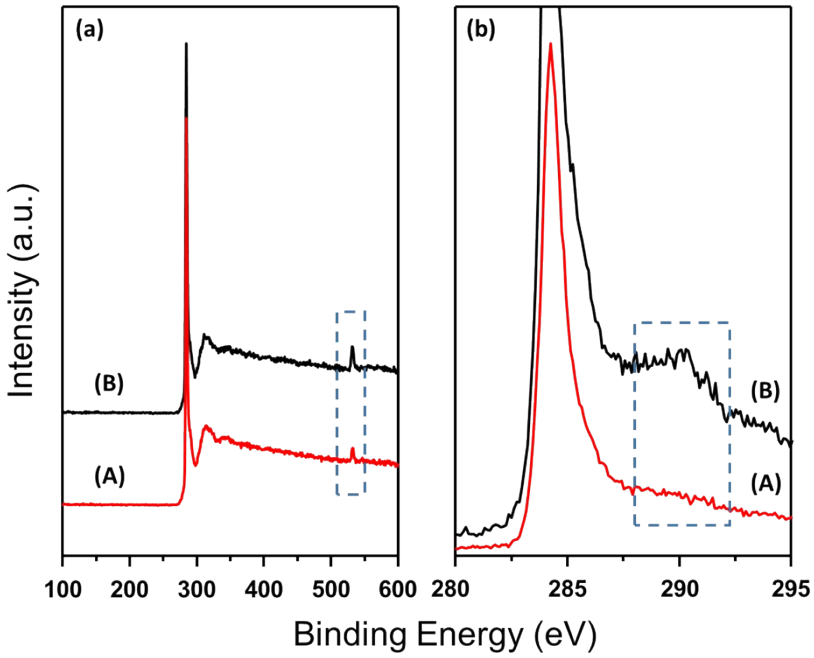

Figure S1. XPS survey spectra (a) and high-resolution XPS C1s spectra (b) obtained for pristine MWCNTs (A) and HNO_3-treated MWCNTs (B).

The types of oxygen-containing groups were investigated and discussed for HNO_3-treated MWCNTs. XPS survey spectra show that pristine MWCNTs and HNO_3-treated MWCNTs mainly contain carbon atoms with a large C1s peak at 284.5 eV except for a small amount of oxygen atoms with an O1s at 531 eV. The O1s peak intensities are significantly enhanced (curves (B) to (A) in Figure S1a), which means that HNO_3 treatment can introduce more oxygen-containing groups on MWCNTs. High-resolution XPS spectra for C1s were measured and shown in Figure S1b. Except for the main peak for sp^2 carbons at 284.5 eV, HNO_3-treated MWCNTs rather than the pristine MWCNTs exhibited a characteristic peak of carboxyl at 289.8 eV, which means that the oxygen-containing groups in HNO_3-treated MWCNTs are mainly -COOH. These carboxyl groups on MWCNTs can be deprotonated into negatively charged groups (ie -COO-) in neutral media, and thus provide the opportunity for adsorption of subsequent Fe cations.

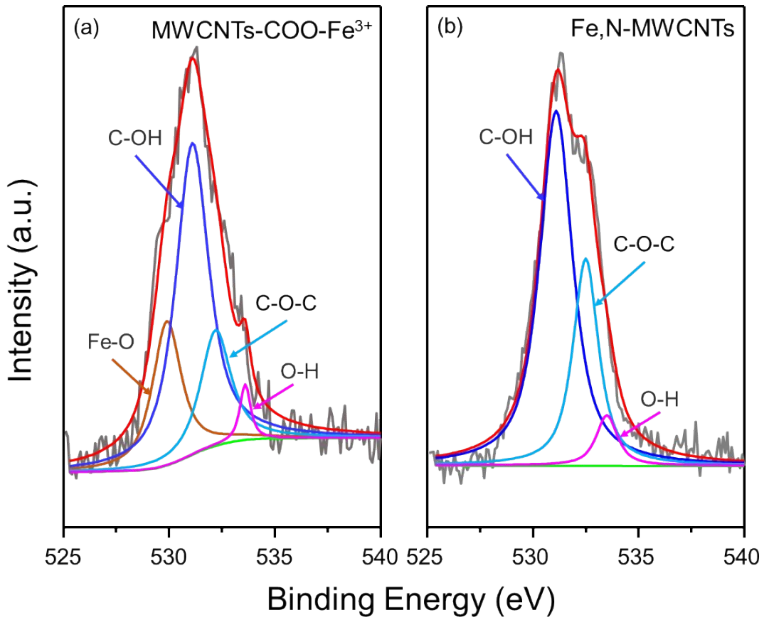

Figure S2. The O1s XPS spectra of MWCNTs-COOFe (a) and Fe,N-MWCNTs (b).

The O 1s XPS spectra of Fe^{3+} adsorbed MWCNTs and Fe,N-MWCNTs were conducted. The O 1s XPS spectra of Fe^{3+} adsorbed MWCNTs can be deconvoluted into four typical peaks: Fe-O bonds (529.9 eV), C-OH bonds (531.8 eV), C-O-C bonds (533.2 eV), and O-H (533.6 eV) [S6, S7], while no obvious Fe-O bonds could be fitted in the O 1s XPS spectra of Fe,N-MWCNTs as shown in Figure S2, strongly suggesting that the Fe-O bonds completely converted to the Fe-N coordination by high temperature.

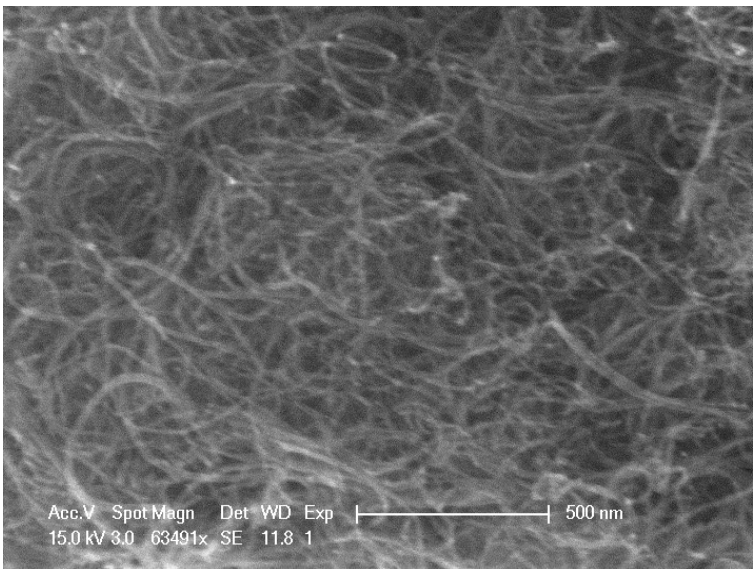

Figure S3. SEM image of pristine MWCNTs.

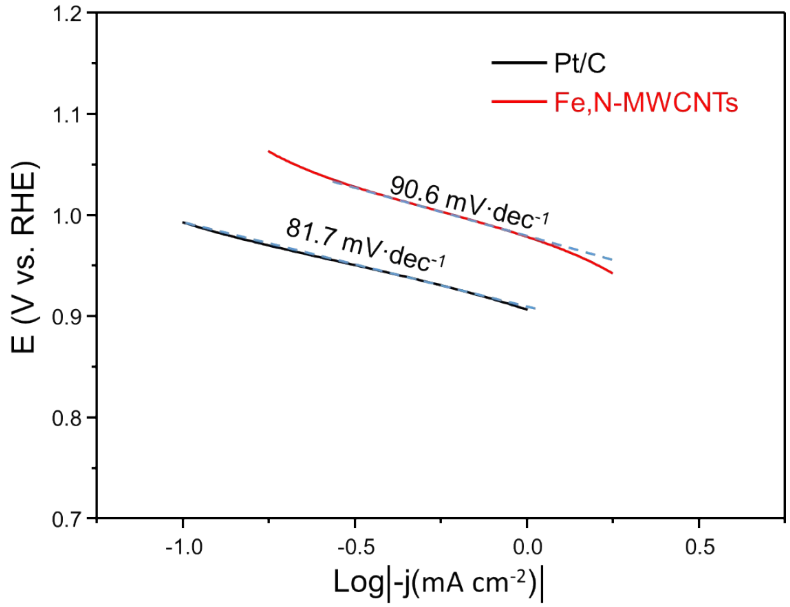

Figure S4. Tafel plots of Fe,N-MWCNTs and Pt/C.

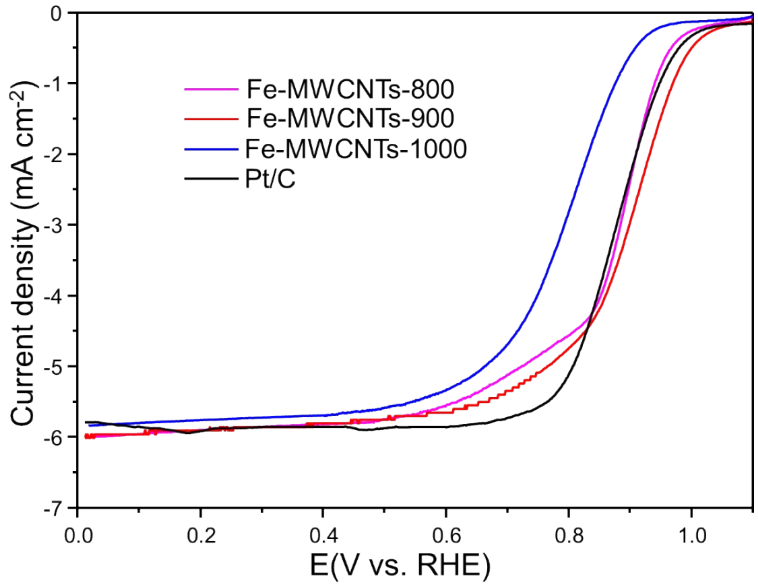

Figure S5. LSV curves of Fe,N-MWCNTs-800/900/1000 and commercial Pt/C at a scanning rate of 10 mV s^{-1} and a rotating speed of 1600 rpm in 0.1 M KOH.

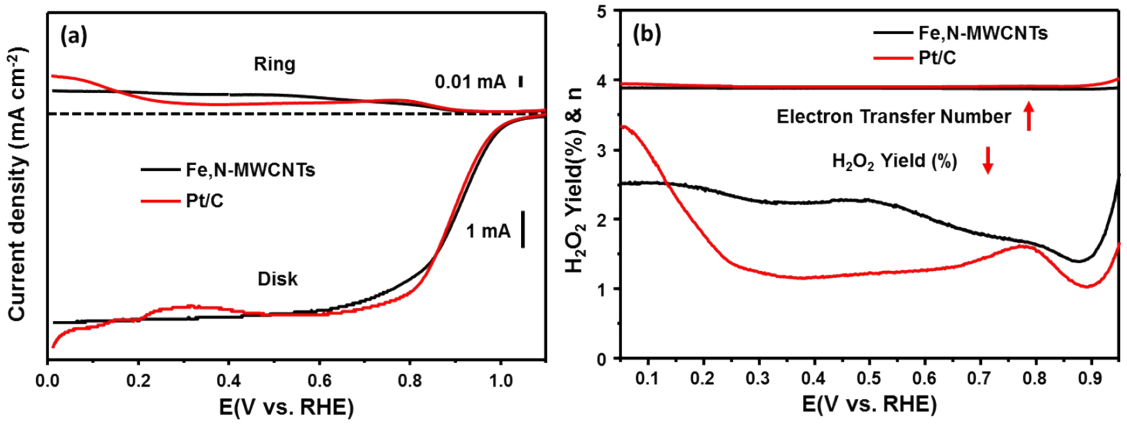

Figure S6. a) LSV curves of Fe,N-MWCNTs and commercial 20% Pt/C catalyst measured on RRDE at 1600 rpm in O_2-saturated 0.1 M KOH. Ring potential: 1.5 V *vs. RHE*; b) The dependence of electron transfer number *n* on the potential and the H_2O_2 generation for the Fe,N-MWCNTs catalyst calculated from the corresponding RRDE data.

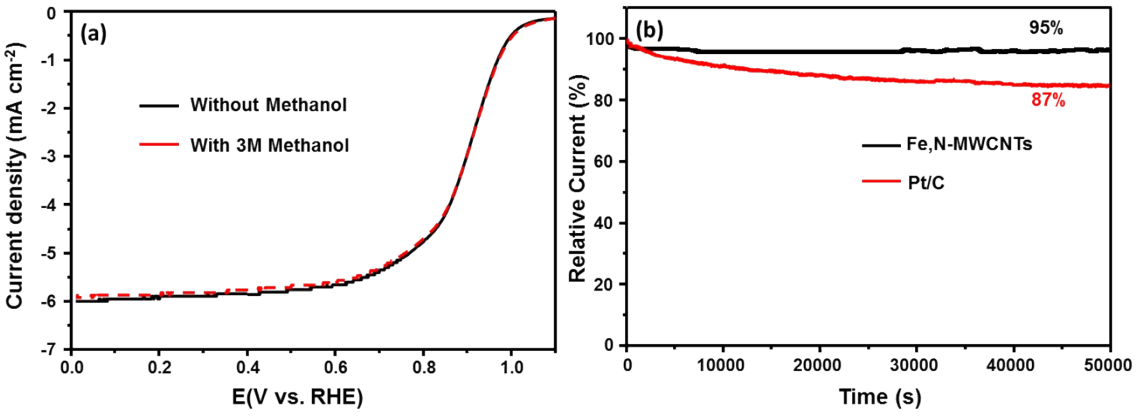

Figure S7. a) The methanol tolerance test of Fe,N-MWCNTs and Pt/C; b) Chronoamperometric curves of Fe,N-MWCNTs and Pt/C at the constant potential of 0.3 V *vs. RHE*.

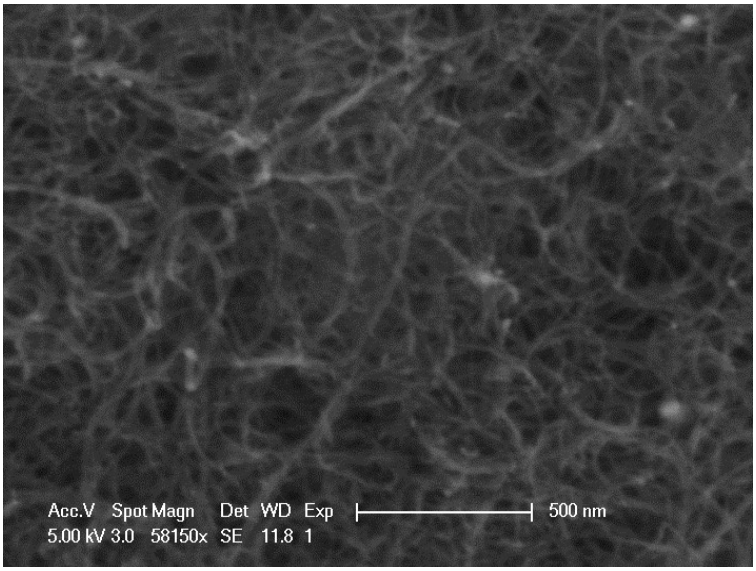

Figure S8. SEM image of Fe,N-MWCNTs after the catalytic stability test.

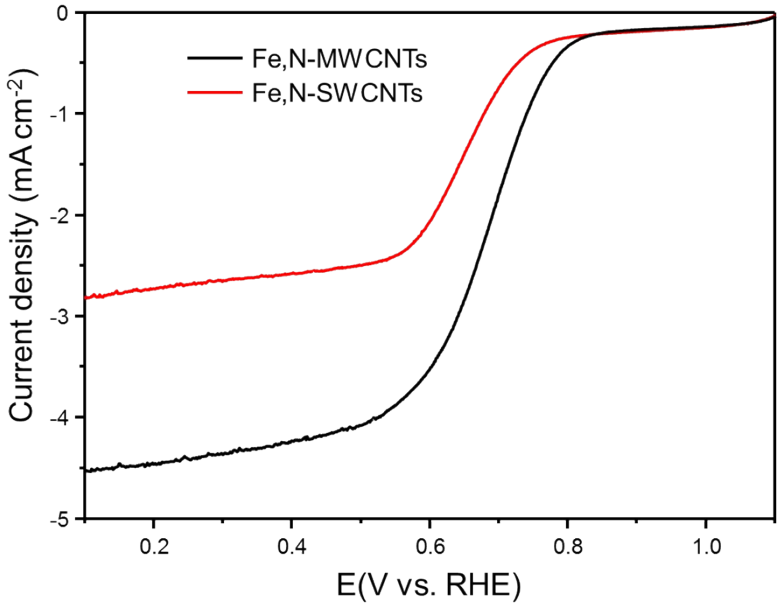

Figure S9. LSV curves of Fe,N-MWCNTs and Fe,N-SWCNTs at a scanning rate of 10 mV s^{-1} and a rotating speed of 1600 rpm in 0.5 M H_2SO_4.

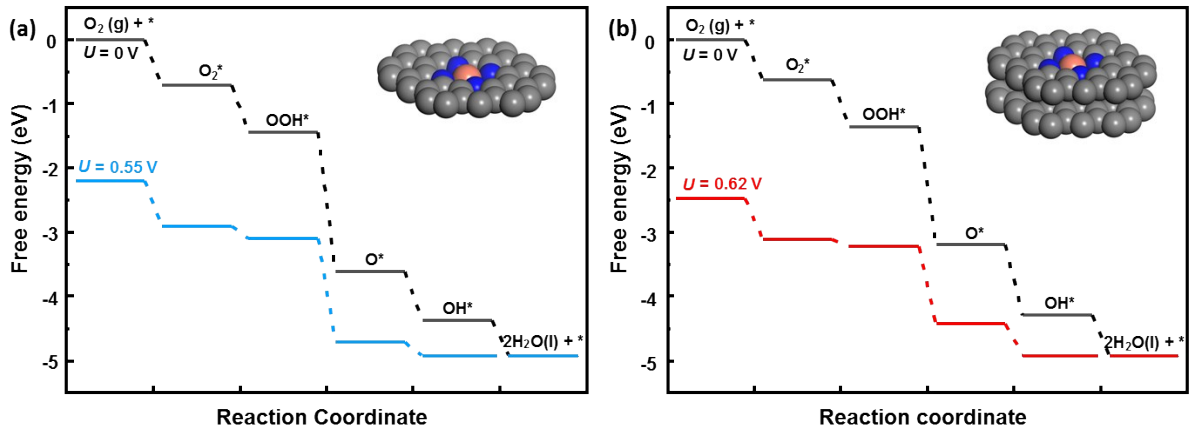

Figure S10. Free energy profiles of ORR on Fe-N sites embedded on (a) single-layer and (b) double-layer carbon layer under acidic condition.

Typically, the four-electron reduction of O_2 of ORR under acidic condition involves the following four steps (after O_2 adsorption)[S8]:

$$O_2* + H^+ + e^- \rightarrow OOH* \quad \text{(R1)}$$

$$OOH* + H^+ + e^- \rightarrow O* + H_2O(l) \quad \text{(R2)}$$

$$O* + H^+ + e^- \rightarrow OH* \quad \text{(R3)}$$

$$OH* + H^+ + e^- \rightarrow H_2O(l) + * \quad \text{(R4)}$$

Figure S5 shows the ORR free energy profiles on Fe-N_4 sites embedded on single and double graphene, respectively. When the electrode potential is 0 V, all the ORR substeps are downhill, and the step (4) shows the lowest free energy downhill on both sites. As show in Figure S5a when the electrode potential rises to 0.55 V, the ΔG of step (4) goes to 0 eV. Thus, the minimum ORR overpotential on the Fe-N_4 site on single-layer carbon is 1.23 – 0.55 = 0.68 V. As for the ORR pathway on the Fe-N_4 site on double-layer graphene (Figure S5b), the maximum electrode potential that keeps all the substeps exothermic is 0.62 V, so the minimum ORR overpotential is 1.23 – 0.62 = 0.61 V. The thermodynamic analysis indicates that the active site with the carbon layer below show the lower overpotential than that without the carbon layer, suggesting the dominant contribution of the carbon layer below the active site to ORR activity.

Table S1. Comparison of ORR catalytic performances in alkaline solution between Fe,N-MWCNTs catalyst and other previously reported catalysts.

Catalyst	E_{onset} (V) [#]	$E_{1/2}$ (V) [^]	Reference
Fe,N-MWCNTs	**1.00**	**0.91**	**This work**
CoFe@C	0.98	0.89	*Angew. Chem.* 2019, 131, 1997.
Co_3O_4/rmGO	0.88	0.83	*Nat. Mater.* 2011, 10, 780
Fe-N/C-800	0.92	0.81	*J. Am. Chem. Soc.* 2014, 136, 11027
Ni/NiO/$NiCo_2O_4$/N-CNT-As	0.89	0.74	*J. Mater. Chem. A* 2016, 4, 6376
CNTs-Co/NHC-0.23	0.98	0.87	*Chem. Commun.* 2018, 54, 11570
Fe_3C@N-CNT	-	0.85	*Energy Environ. Sci.* 2016, 9, 3092
CoZn-NC-700	-	0.84	*Adv. Funct. Mater.* 2017, 27, 1700795
NPMC-1000	0.94	0.85	*Nat. Nanotechnol.* 2015, 10, 444
Co@N-CNTs-m	0.97	0.87	*Carbon* 2016, 107, 162
$NiCo_2S_4$@g-C_3N_4-CNT	0.87 V	0.76	*Adv. Mater.* 2019, 31, 1808281

[#] E_{onset} is the onset potential of ORR. All the potentials are *versus* the RHE.

[^] $E_{1/2}$ is the half-wave potential of ORR. All the potentials are versus the RHE.

Table S2. Results of chemical composition analysis from XPS measurements for the catalysts prepared at different pyrolysis temperatures.

Samples	Fe,N-MWCNTs-800	Fe,N-MWCNTs-900	Fe,N-MWCNTs-1000
At% (C)	85.85	85.94	90.23
At% (N)	4.45	4.39	3.17
At% (Fe)	0.22	0.24	0.16
At% (O)	9.48	9.43	6.44

References

[S1] G. Kresse and J. Furthmüller, *Phys. Rev. B*, 1996, **54**, 11169.

[S2] J.P. Perdew, K. Burke and M. Ernzerhof, *Phys. Rev. Lett.*, 1996, **77**, 3865-3868.

[S3] G. Kresse and D. Joubert, *Phys. Rev. B*, 1999, **59**, 1758.

[S4] J.K. Nørskov, J. Rossmeisl, A. Logadottir, L. Lindqvist, J.R. Kitchin, T. Bligaard and H. Jonsson, *J. Phys. Chem. B*, 2004, **108**, 17886-17892.

[S5] C. Guo, T. Zhang, X. Deng, X. Liang, W. Guo, X. Lu and C.-M.L. Wu, *ChemSusChem*, 2019, **12**, 5126-5132.

[S6] M. Ma, S. You, W. Wang, G. Liu, D. Qi, X. Chen, J. Qu and N. Ren, *ACS Appl. Mater. Interfaces*, 2016, **8**, 32307-32316.

[S7] Z. Guo, Z. Xiao, G. Ren, G. Xiao, Y. Zhu, L. Dai and L. Jiang, *Nano Rev.*, 2016, **9**, 1244-1255.

[S8] X. Guo, S. Lin, J. Gu, S. Zhang, Z. Chen and S. Huang, *ACS Catal.*, 2019, **9**, 11042-11054.